# Flow physics of a passive flap on a dynamically pitched airfoil

Zoey Flynn \* and Andres Goza † University of Illinois at Urbana-Champaign, Urbana, Illinois, 61801

Covert bird feathers are believed to passively deploy during flight to mitigate separation effects and improve aerodynamic performance, contributing to these animals' maneuverability even in unsteady conditions. Engineered devices that can mimic this effect have the potential to aid flight robustness and performance in next generation vehicles. We numerically investigate a canonical representation of this covert-feather system by mounting a thin, rigid flap to an airfoil via a torsional hinge. This configuration is known to be capable of significantly increasing the mean lift for a stationary airfoil at a stalled angle of attack. Yet, there remain open questions about the benefits associated with using this flap on an airfoil undergoing unsteady maneuvers and the mechanisms responsible for these benefits. In this study we use high-fidelity fully coupled fluid-structure interaction simulations to investigate the behaviors of a flap mounted via a torsional spring on an airfoil undergoing a pitch-up maneuver from  $\alpha = 0-45^{\circ}$ . We perform a 2D numerical investigation at a Reynolds number of Re = 1,000 with the torsional flap located at 0.4 chord lengths, measured from the leading edge of the flap. Results indicate that the torsional flap greatly increases lift at the start of the pitch-up motion due to the formation of a clockwise vortex just downstream of the flap. However, the flap also appears to cause a loss in lift at the end of pitch-up by a premature downstream advection of the clockwise vortex. In total, the flap increases the total generated lift throughout the pitch-up maneuver by approximately 5%.

## I. Nomenclature

 $a_s$  = pitching parameter

c = chord

 $i_{\beta}$  = flap moment of inertia

K = nominal pitch rate

 $k_{\beta}$  = flap stiffness

 $l_{\beta}$  = flap position

p = pressure

Re = Reynolds number

s = surface parameter

t = time

 $U_{\infty}$  = freestream velocity

u = flow velocity

x =fluid grid points

 $x_c$  = airfoil center of rotation

 $\alpha$  = angle of attack

 $\alpha_0$  = maximum angle of attack

 $\dot{\alpha}_0$  = nominal angular velocity

 $\beta$  = flap deflection angle

 $\Gamma$  = body coordinate system

 $\Delta T_h$  = holding time

 $\Delta t$  = time step

 $\Delta x$  = grid spacing

= kinematic viscosity

<sup>\*</sup>Graduate Research Assistant, Department of Aerospace Engineering

<sup>&</sup>lt;sup>†</sup>Assistant Professor, Department of Aerospace Engineering, AIAA Member

 $\rho_f$  = fluid density

 $\chi$  = immersed body points

 $\chi_a$  = airfoil body points

 $\chi_f$  = flap body points

 $\chi_f^0$  = flap hinge location

 $\Omega$  = fluid coordinate system

## **II. Introduction**

Birds have the remarkable ability to perform aerodynamic maneuvers at high angles of attack and a wide range of Reynolds numbers; a feature that is difficult but necessary to duplicate in next-generation aircraft. Studies of bird flight have shown that this maneuverability may be aided by the covert feathers along the upper surface of the bird's wings. During unsteady flight conditions (such as landing or take off) the coverts deflect from the wing in such a way that indicates it is a passive response to separation in the surrounding flow [1].

Many efforts have been made to mimic the behavior of coverts in passive flow control devices. These studies often consider thin flaps mounted to the airfoil, either at a fixed deflection angle or freely moving with a hinge. Experiments show that while the addition of these flaps does produce a small detrimental increase in drag and decrease in lift pre-stall, well positioned flaps can both delay stall and reduce the loss in lift post-stall by a significant amount [2–4]. This is largely due to the configuration of the flap, which prevents reverse flow from traveling upstream along the surface of the airfoil [5]. Greater benefits can be attained by mounting the flap via a finite stiffness torsional hinge. Unlike a freely hinged flap, which can over deploy during separation, the spring force limits motion in a manner more accurate to real covert feathers. Rosti et al. [6] demonstrated numerically that the use of a finite stiffness torsional spring can lead to additional benefits compared with the free (zero-stiffness) case, which the authors linked to structural resonance, using an in-vacuo scaling that neglected added mass effects. Nair and Goza [7, 8] numerically performed a broader sweep of flap parameters and found that the behavior of the torsional flap can be classified into different flow regimes depending on whether it primarily interacts with the shear layer or the shed vortices. In both cases, the flap is capable of significantly improving the mean lift for certain stiffness and inertia values. The authors found that the largest benefits were obtained through a balance between aligning the flap resonance (with appropriately defined added mass terms) near the intrinsic vortex shedding frequency and retaining an appropriate mean configuration, encoded by the flap stiffness [8].

Nevertheless, there are still many questions about the behavior of these flaps, especially under dynamic motion. Much of the existing literature focuses on airfoils at a fixed post-stall angle of attack. But any practical implementation of these torsional flaps will require a more complete understanding of their behavior over the full development of unsteady flow. A recent numerical study by Rosti et al. [9] observed that the addition of a torsional flap to a dynamically pitching airfoil improved the aerodynamic efficiency and delayed stall. Similar to the static airfoil configuration, the presence of the torsional flap limits direct interaction between the leading and trailing edge flow, which delays the dynamic stall process. The flap's motion also causes the trailing-edge vortex to advect downstream earlier than the reference case so the dynamic stall leading-edge vortex stays attached longer. Similar to the stationary airfoil case, the authors linked maximal benefits to having flap parameters with an in-vacuo structural natural frequency equal to the frequency of vortex shedding. Yet, it is still unclear how factors such as the flap inertia and stiffness can individually influence the airfoil's performance under these conditions. Moreover, it is unknown how the flow regimes identified in Nair and Goza [7] are affected by the dynamic motion. Finally, the dynamic airfoil motion yields non-stationary dynamics (inexpressible through frequency decompositions), and quantifying the flap-flow mechanisms in terms of these transient processes remains unexplored.

In this work we perform a numerical investigation of a dynamically pitching NACA 0012 airfoil with a torsional flap. The airfoil is subjected to a nominally linear pitch-up maneuver from  $0^{\circ}$  to  $45^{\circ}$ . It is modeled in a uniform 2D flow with Reynolds number Re = 1000. The flap is positioned at a distance 0.4c along the upper surface of the airfoil with a fixed stiffness and inertia.

## III. Problem Setup

For this study we use a NACA 0012 airfoil simulated in a uniform flow with freestream velocity  $U_{\infty}$  and chord Reynolds number Re = 1000. Figure 1 illustrates the airfoil setup. The airfoil has nondimensional chord length c and a center of rotation at  $x_c = 0.25c$  along its chord line. A flap of length 0.2c is mounted along the upper suction surface of

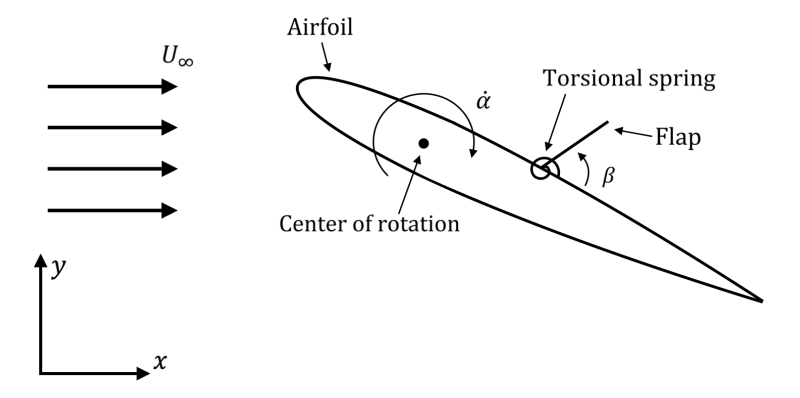


Fig. 1 Schematic of the torsionally hinged flap mounted on a NACA 0012 airfoil.

the airfoil with a torsional hinge that allows it to deploy freely into the flow. The flap is initially deployed at an angle of  $5^{\circ}$  relative to the surface of the airfoil to allow it to properly deploy without collisions against the airfoil. The flap has a prescribed nondimensional spring stiffness,  $k_{\beta}$ , and moment of inertia,  $i_{\beta}$ . The nondimensional position of the flap hinge is denoted  $l_{\beta}$  relative to the leading-edge of the airfoil. These parameters are given as

$$i_{\beta} = \frac{I_{\beta}}{\rho_f c^4}, \quad k_{\beta} = \frac{K_{\beta}}{\rho_f U_{\infty}^2 c^2}, \quad l_{\beta} = \frac{L_{\beta}}{c}, \tag{1}$$

where  $I_{\beta}$ ,  $K_{\beta}$ , and  $L_{\beta}$  are the dimensional inertia, stiffness, and flap position respectively. For this study we focus on one case with  $k_{\beta} = 0.01$ ,  $i_{\beta} = 0.01$ , and  $l_{\beta} = 0.4$ . The variable  $\rho_f$  is the density of the fluid.

$$\alpha(t) = \alpha_0 \frac{G(t)}{\max(G(t))},\tag{2}$$

$$G(t) = \log \left( \frac{\cosh(a_s(t - t_1))\cosh(a_s(t - t_4))}{\cosh(a_s(t - t_2))\cosh(a_s(t - t_3))} \right).$$
(3)

The motion of the airfoil is prescribed using a smooth pitching function from Eldredge and Wang [10]. Equation 2 describes a pitch-up motion, from time  $t_1$  to  $t_2$ , followed by a holding period, and then a pitch-down motion from  $t_3$  to  $t_4$ . For the purposes of this study we only focus on the pitch-up motion, which is displayed in Figure 3. Note that all times are nondimensionalized by  $U_{\infty}/c$ . The airfoil rotates at angular velocity  $\dot{\alpha}_0 = 2K\frac{U_{\infty}}{c}$  with nominal pitch rate K = 0.2. The time intervals are therefore defined by

$$t_2 = t_1 + \frac{\alpha_0}{\dot{\alpha}_0}, \quad t_3 = t_2 + \Delta T_h, \quad t_4 = t_3 + \frac{\alpha_0}{\dot{\alpha}_0}.$$
 (4)

 $\Delta T_h$  is the hold time between the end of pitch-up and the start of pitch-down. For this study we set  $a_s = 11$ ,  $t_1 = 1$ ,  $\Delta T_h = 1.12$ , and  $\alpha_0 = 45^{\circ}$ .

## IV. Numerical Methodology

We model the problem with the immersed boundary method described in Nair and Goza [11]. In this approach, the fluid domain is assigned an Eulerian coordinate system,  $\Omega$ , and the immersed body is assigned a Lagrangian coordinate system,  $\Gamma$ . The flow points in  $\Omega$  are denoted by x and the body points in  $\Gamma$  are defined by  $\chi$ . We utilize the variable s to parameterize the surface of the immersed bodies. All position coordinates are nondimensionalized by the chord length. We also define the fluid velocity, u, which is nondimensionalized by  $U_{\infty}$ . The governing equations for the fluid-structure interaction system are

$$\frac{\partial \mathbf{u}}{\partial t} + \mathbf{u} \cdot \nabla \mathbf{u} = -\nabla p + \frac{1}{Re} \nabla^2 \mathbf{u} + \int_{\Gamma} f(\chi(s,t)) \delta(\chi(s,t) - \mathbf{x}) ds, \tag{5}$$

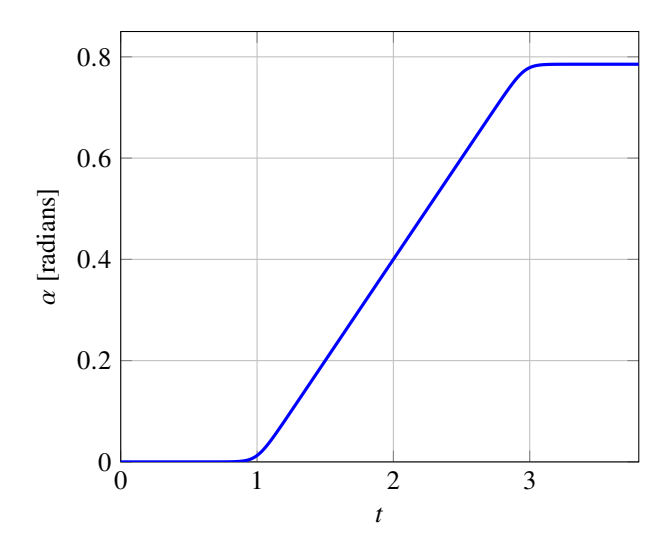


Fig. 2 The angle of attack for the airfoil begins at  $\alpha = 0$  and increases linearly until it reaches  $\alpha_0$ .

$$\nabla \cdot \boldsymbol{u} = 0, \tag{6}$$

$$i_{\beta} \frac{\partial^{2} \beta}{\partial t^{2}} + k_{\beta} \beta = -\int_{\Gamma_{f}} (\chi_{f} - \chi_{f}^{0}) \times f(\chi_{f}) d\chi_{f}, \tag{7}$$

$$\int_{\Omega} u(\mathbf{x})\delta(\mathbf{x} - \chi_a)d\mathbf{x} = 0,$$
(8)

$$\int_{\Omega} \boldsymbol{u}(\boldsymbol{x})\delta(\boldsymbol{x} - \boldsymbol{\chi}_f)d\boldsymbol{x} = \frac{\partial \beta}{\partial t}\hat{\boldsymbol{e}}^i \times (\boldsymbol{\chi}_f - \boldsymbol{\chi}_f^0). \tag{9}$$

Equation 5 is the Navier Stokes Equation. It contains the nondimensional pressure and chord Reynolds number which are written below. In the Reynolds number,  $\nu$  is the kinematic viscosity. Additionally,  $f(\chi)$  represents the surface stresses on the body.

$$p = \frac{P}{\rho_f U_{\infty}^2}, \quad Re = \frac{U_{\infty}c}{\nu}. \tag{10}$$

Equation 6 is the continuity condition for incompressible flow. Equation 7 describes the motion of the flap. In this equation,  $\beta$  is the flap deflection angle and  $\chi_f$  refers to the body points of the flap only. Additionally,  $\chi_f^0$  is the location of the flap's hinge. Equations 8 and 9 are the no slip conditions for the airfoil and flap respectively.  $\chi_a$  refers to the body points of the airfoil and  $\hat{e}^i$  is the unit direction vector for the angular motion of the flap.

The flow equations 5 and 6 are spatially discretized using the standard second-order central difference scheme. For temporal discretization, an Adams Bashforth 2-step scheme is used for the advection term and a trapezoid scheme is used for the diffusive term. Equation 7 is discretized in time with a Newmark scheme. The nonlinear algebraic system is solved using a Newton iteration method, with a block-LU factorization used to restrict FSI iterations to systems that scale with the number of points used to discretize the structure, rather than the (far greater) number of points used to represent the entire flow and structural domain. Additionally, a sub-domain approach is used to pre-compute the fluid-structure coupling matrices that arise from the LU factorization. The pre-computed matrices allow for an embedded linear solve, that scales with the total number of points in the flow domain, to be avoided at substantial computational savings. See Nair and Goza [11] for more details.

For all results below, we use a time step of  $\Delta t = 0.0004375$  and a grid spacing of  $\Delta x = 0.00349$ . These values are consistent with those used by Nair and Goza [8] for a stationary airfoil case, and for the modest pitch rate chosen below the flow velocity magnitudes are commensurate with that study.

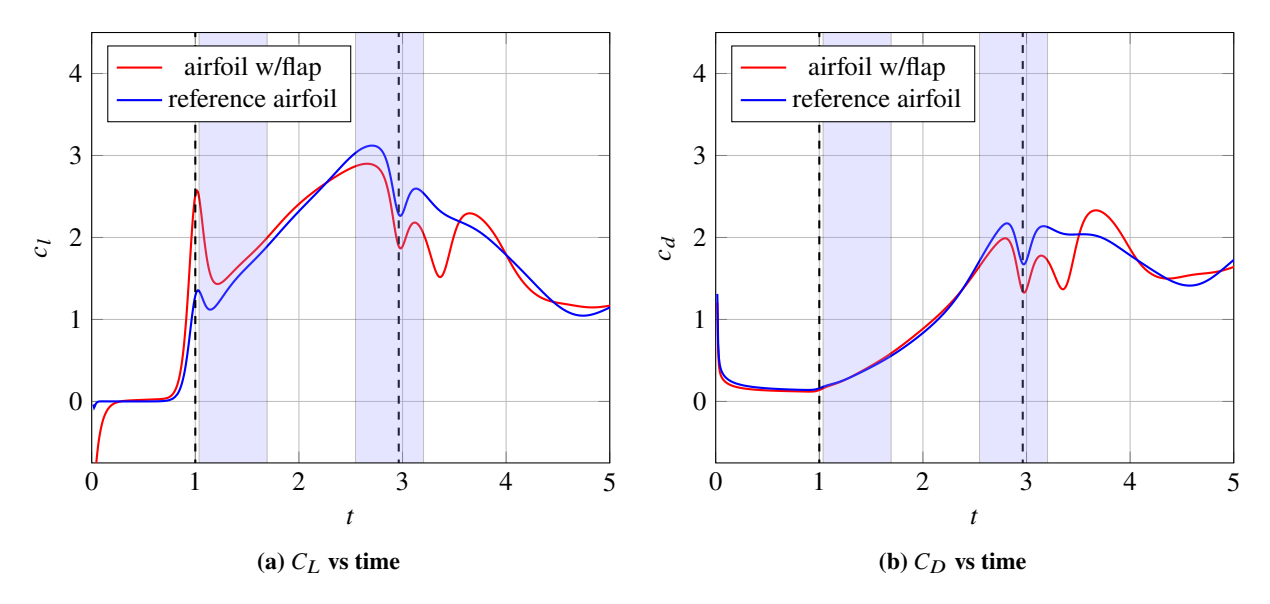


Fig. 3 Lift (left) and drag (right) coefficients on the airfoil body throughout the pitch-up motion showing that the airfoil with the flap follows the same trends as the reference but with significantly exaggerated features. The vertical dashed lines represent the start and end times of pitch-up and the light blue regions indicate the time interval in which the flow snapshots analyzed later in the manuscript have been taken.

#### V. Results

First we examine the reference case for the airfoil with no flap. Figure 3a shows the development of the lift coefficient over the full pitching motion. There is a clear peak in the lift around t = 1, which is the inertial reaction to the start of pitch-up [10]. As the airfoil continues to rotate, the lift increases in a near-linear fashion until we observe a sharp decrease in lift near t = 3, just before the pitching motion ends. The drag coefficient, by contrast, increases smoothly throughout the start of pitch-up, as shown in Figure 3b. There is no inertial reaction at the start of pitching, but there is a decrease in drag just before pitch-up ends.

The case of the airfoil equipped with a torsional flap shares many of the same lift and drag features as the reference case; there is a large lift increase at the start of pitch-up and a sharp decrease in both lift and drag near the end. However, in the flap case, these features are significantly more pronounced. There is also more variation in the slope of the lift, with  $C_L$  being higher in the flap case for the first half of pitching but then dropping below that of the reference case for the latter half. This results in the airfoil with the flap having a 5% improvement in total integrated lift over the full pitch-up maneuver (t = 0.75 - 3).

These effects are caused by the flap, which alters the vortex dynamics throughout the pitching motion. Figure 4 shows the vorticity around the airfoil for several time steps around t = 1. A lift-producing (clockwise) vortex forms just downstream of the flap directly after pitching begins, leading to higher lift via a low pressure area that grows with the vortex. There is no analogous vortex on the reference airfoil during this time period, hence the smaller lift coefficient.

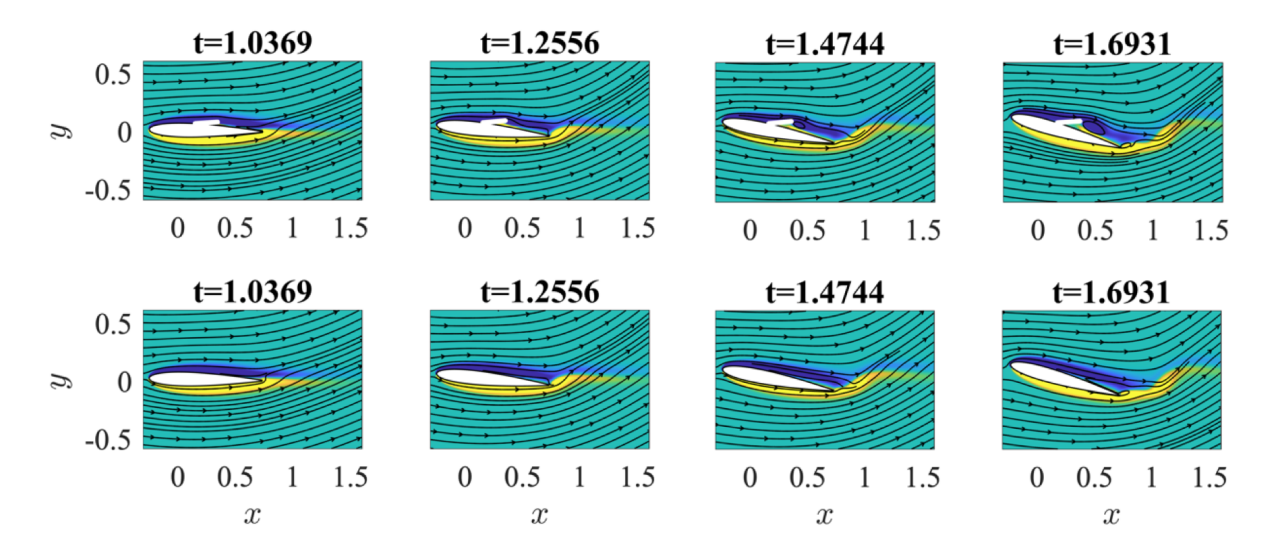


Fig. 4 Vorticity and pressure near the start of pitch-up for the airfoil with the flap (top) and the reference case (bottom).

Figure 5 shows vorticity plots for the end of pitch-up around t = 3. For the reference case with no flap, there are two flow features beginning to form around t = 2.5: a leading-edge vortex (LEV) and a secondary clockwise vortex just upstream of the trailing edge. In the flap case, there is also an LEV but the secondary clockwise vortex is replaced by the clockwise vortex that previously formed downstream of the flap. As a result, the secondary vortex in the flap case is significantly larger than the one in the reference case at t = 2.5 since it developed much earlier. The LEV and secondary vortex continue to grow for the remainder of pitch-up. At every time instance the LEVs are nearly identical in size but the secondary vortex is always larger in the flap case, indicating that its growth is responsible for the change in lift at the end of pitch-up.

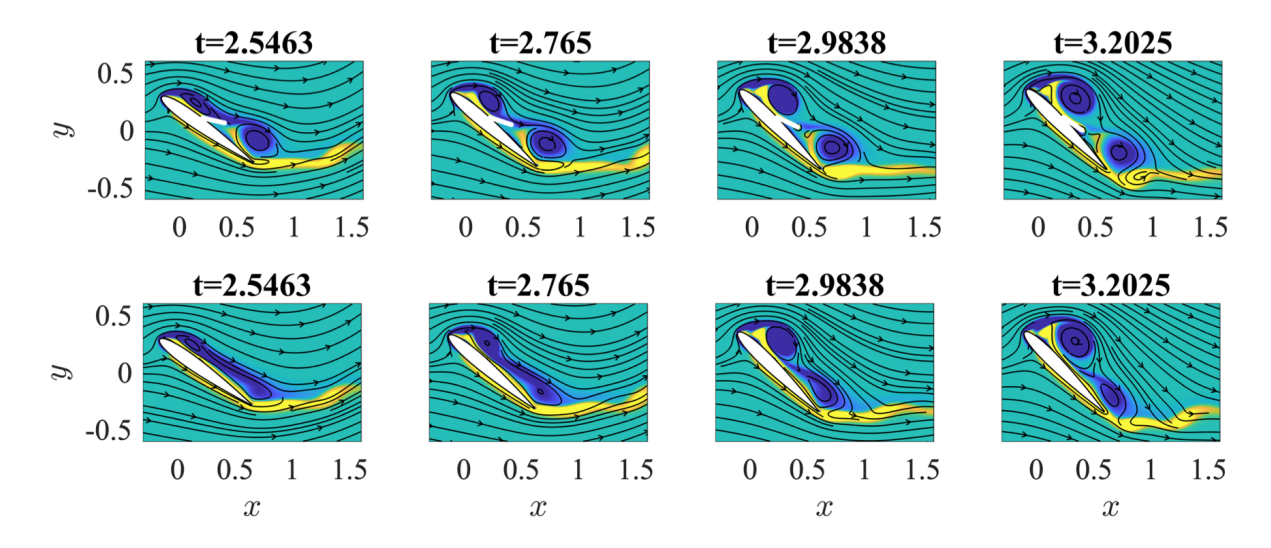


Fig. 5 Vorticity and pressure near the end of pitch-up for the airfoil with the flap (top) and the reference case (bottom).

Closer observation of the secondary vortex in the flap case shows that a small region of reverse flow has formed underneath the vortex. This region is also present in the reference case with no flap, but it is larger and has begun to roll up with the secondary vortex in the flap case. This roll-up behavior could be attributed to the natural growth of the secondary vortex, but is also influenced by (1) the presence of the flap, which is deployed just enough to block a

portion of reverse flow from traveling upstream; and (2) the motion of the flap, which closes towards the airfoil surface from t = 2.5 - 3.3 (c.f., Figure 6). The latter effect imposes a jet-like momentum forcing on the secondary vortex downstream, which allows more reverse flow up the airfoil.

We briefly note from the lift curve in Figure 3a that the  $C_L$  values are quite different between the flap and flap-less cases during the post pitching period. There is a sharp drop in lift for the flap case at t=3.3 that is not present in the reference case. This behavior is followed by short discrete periods of lift improvement, correlated with the LEV advecting downstream. Commensurate with the downstream advection and interaction of these flow features, figure 6 shows a sudden deployment of the flap to a much larger angle. The focus in this article is the fluid-structure interaction that occurs during the pitch process; the complex interplay post-pitch is a subject of future study.

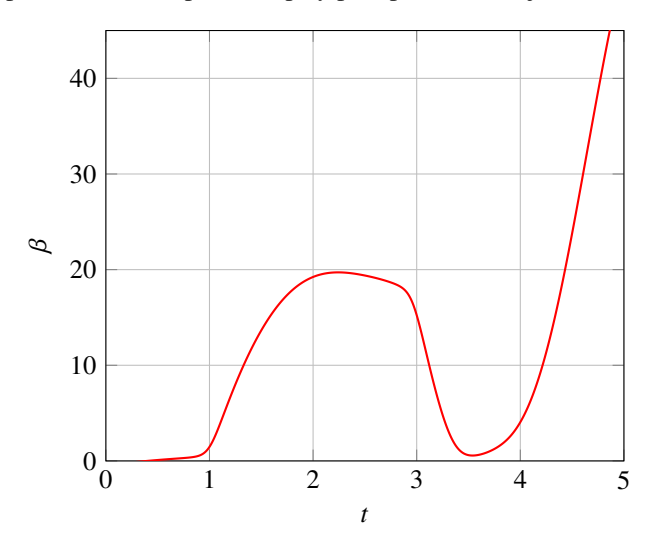


Fig. 6 Flap deflection over time during the pitch-up maneuver relative to the surface of the airfoil.

# VI. Conclusions

We performed high-fidelity fully coupled fluid-structure interaction simulations of a bio-inspired flap hinged by a torsional spring onto an airfoil undergoing a pitch-ramp maneuver. The results demonstrate that the flap was able to generate a 5% increase in lift during the pitch process. The flap yields a significant lift increase near the start of pitch-up by causing a lift-producing vortex to form much earlier during the pitching motion (compared with the flap-less case). Conversely, the early growth of this vortex leads to an early advection at the end of pitch-down which results in a loss of lift during that time interval compared with the flap-less case. Nevertheless, the flap yielded an overall lift improvement during the pitch process at a negligible expense of additional drag. This outcome indicates that these bio-inspired flaps have benefits as passive, adaptive control strategies during dynamic airfoil motions.

## VII. Acknowledgements

The authors gratefully acknowledge funding from NSF CBET under award number 20-29028.

#### References

- [1] Carruthers, A., Thomas, A., and Taylor, G., "Automatic aeroelastic devices in the wings of a steppe eagle Aquila nipalensis." *Journal of Experimental Biology*, Vol. 210, No. 23, 2007, pp. 4136–4149.
- [2] Allemand, G., and Altman, A., "Post-Stall Performance Improvement through Bio- inspired Passive Covert Feathers," 54th AIAA Aerospace Sciences Meeting, 2016, p. 2042.
- [3] Kernstine, K., Moore, C., Cutler, A., and Mittal, R., "Initial Characterization of Self-Activated Movable Flaps," Pop-Up Feathers"," 46th AIAA Aerospace Sciences Meeting and Exhibit, 2008, p. 369.
- [4] Meyer, R., Hage, W., Bechert, D. W., Schatz, M., Knacke, T., and Thiele, F., "Separation Control by Self-Activated Movable Flaps," *AIAA Journal*, Vol. 45, No. 1, 2007, pp. 191–199.

- [5] Duan, C., and Wissa, A., "Covert-inspired flaps for lift enhancement and stall mitigation," *Bioinspiration & Biomimetics*, Vol. 16, No. 4, 2021.
- [6] Rosti, M. E., Omidyeganeh, M., and Pinelli, A., "Numerical Simulation of a Passive Control of the Flow Around an Aerofoil Using a Flexible, Self Adaptive Flaplet," *Flow, Turbulence and Combustion volume*, Vol. 100, 2018, p. 1111–1143.
- [7] Nair, N. J., and Goza, A., "Effects of Torsional Stiffness and Inertia on a Passively Deployable Flap for Aerodynamic Lift Enhancement," *AIAA SCITECH 2022 Forum*, 2022, p. 1968.
- [8] Nair, N. J., and Goza, A., "Fluid-structure interaction of a bio-inspired passively deployable flap for lift enhancement," *arXiv* preprint arXiv:2203.00037, 2022.
- [9] Rosti, M. E., Omidyeganeh, M., and Pinelli, A., "Passive control of the flow around unsteady aerofoils using a self-activated deployable flap," *Journal of Turbulence*, Vol. 19, No. 3, 2017, pp. 204–228.
- [10] Eldredge, J. D., and Wang, C., "High-Fidelity Simulations and Low-Order Modeling of a Rapidly Pitching Plate," 40th Fluid Dynamics Conference and Exhibit, 2010, p. 4281.
- [11] Nair, N. J., and Goza, A., "A strongly coupled immersed boundary method for fluid-structure interaction that mimics the efficiency of stationary body methods," *Journal of Computational Physics*, Vol. 454, 2022, p. 110897.